INVESTIGATION OF THE MAGNETIC PROPERTIES AND MAGNETOCALORIC EFFECT OF $ZnFe_3C$ ANTIPEROVSKITE: MEAN-FIELD THEORY

H. KERRAI[1], M. SALAMA[2], E. M. JALAL[2,3,a], H. SAADI[2], A. ZAIM[1], M. KEROUAD[1]

[1]Physics of Materials and Systems Modeling Laboratory (PMSML), Unit Associated at CNRST-URAC: 08, Faculty of Sciences, Moulay Ismail University, Meknes, Morocco

[2]Theoretical Physics Team, Laboratory of Condensed Matter Physics, Faculty of Sciences, Chouaib Doukkali University, El Jadida, Morocco

[3]LS2ME Laboratory, Polydisciplinary Faculty of Khouribga, Sultan Moulay Slimane University, Beni Mellal, Morocco

Corresponding author[a]: elmostafa.jalal@usms.ma

Received March 14, 2025

Abstract. In this study, the magnetic, magnetocaloric, and hysteresis properties of the anti-perovskite compound $ZnFe_3C$ were investigated using a mean-field approximation. The results demonstrate that the magnetization gradually decreases with increasing temperature. Conversely, the application of an external magnetic field enhances the alignment of magnetic moments, leading to an increase in the critical temperature (T_c). The magnetic entropy change ($-\Delta S_m$) exhibits a distinct peak at T_c, while the relative cooling power (RCP) shows a linear increase. Additionally, hysteresis analysis reveals that both coercivity and remanence progressively diminish as the temperature rises, with the hysteresis loop disappearing above T_c, indicating a transition to the paramagnetic phase. These findings highlight the potential of $ZnFe_3C$ as a promising material for sustainable, high-performance magnetic refrigeration applications.

Key words: Anti-perovskite, $ZnFe_3C$, Mean-field approximation, Magnetocaloric effect, Hysteresis behavior.

DOI: https://doi.org/10.59277/RomJPhys.2025.70.613

1. INTRODUCTION

The increasing demand for environmentally friendly and energy-efficient solutions has propelled research and application of magnetic refrigeration materials to the forefront as a critical pathway to address the limitations of traditional refrigeration technologies [1–3]. Magnetic refrigeration technology, a novel approach, offers advantages such as high energy conversion efficiency, environmental sustainability, compact design potential, and reliable operation, making it a leading candidate to replace conventional gas compression/expansion refrigeration in the future [4, 5]. The magnetocaloric effect (MCE), first observed by Warburg in 1881 [6], describes the heating or cooling of magnetic materials under a varying magnetic field. This effect is central to magnetic refrigeration cycles, which rely on magnetic solids exhibiting significant MCE, low thermal and magnetic hysteresis, and other essential properties for efficient operation [7]. Extensive research has been conducted on utilizing the MCE in magnetic solids for cooling applications. Magnetic refrigeration materials are typically classified into second-order transition (SOT) and first-order transition (FOT) materials based on their phase transition behavior [8]. FOT materials, such as $MnFeP_{1-x}As_x$ [10], $LaFe_{11.4}Si_1.6$ [11], $Gd_5Si_2Ge_2$ [9], and $MnAs_{1-x}Sb_x$ [12], often demonstrate large magnetic entropy changes ($-\Delta S_M$) but are constrained by a narrow temperature range, significant hysteresis, and magnetic losses, which limit their practical efficiency. In contrast, SOT materials, while exhibiting lower magnetic entropy changes, display excellent reversibility with respect to temperature and magnetic field [13].

Recent advancements have identified numerous SOT materials, including RE_2CoTiO_6 [16], $Ho_{0.2}Tm_{0.2}Gd_{0.2}Co_{0.2}Al_{0.2}$ [14], $Gd(Fe_{0.25}Ni_{0.25}Al_{0.25}Cr_{0.25})O_3$ [18], Ho_3Pd_2 [15], $Gd_{63}Ni_{37}$ [19], $Al_{1-x}Si_xFe_2B_2$ [17], $Gd_2Ti_2O_7$ [20], and GdCoC [21], which exhibit significant reversible MCEs and high refrigerant capacity (RC) values across broad temperature ranges. Recent studies have explored the magnetocaloric properties of various materials. For instance, Chen *et al.* [22] investigated the magnetocaloric and magnetic phase transition characteristics of PrZnSi and NdZnSi compounds, which crystallize in an AlB_2-type hexagonal structure. These materials exhibited second-order magnetic phase transitions at ordering temperatures of 13.5 K and 18.5 K, respectively, with magnetocaloric parameters reaching up to 16.3 J/kg.K for PrZnSi and 15.4 J/kg.K for NdZnSi under a 0–7 T magnetic field. Similarly, other investigations have focused on oxide perovskites, examining their structural, magnetic, and magnetocaloric properties for active cooling applications [23–28].

Among anti-perovskite compounds, $ZnFe_3C$ stands out due to its metallic behavior and exceptional magnetic properties. Studies have revealed a significant overlap between its valence and conduction bands, confirming its metallic character, particularly when analyzed using the generalized gradient approximation (GGA) [29]. Monte Carlo simulations have demonstrated that $ZnFe_3C$ undergoes a second-order phase transition from the ferromagnetic to the paramagnetic state, accompanied by a high Curie temperature. These properties make $ZnFe_3C$ a promising candidate for magnetic refrigeration systems and magnetic sensor development. A deeper understanding of its electronic and magnetic properties further reinforces its potential for next-generation magnetic devices.

To date, the mean-field approximation based on the Gibbs-Bogoliubov inequality has not been applied to study the magnetic properties, magnetocaloric effect, and hysteresis behavior of $ZnFe_3C$. This study aims to theoretically explore the fundamental properties of the anti-perovskite compound $ZnFe_3C$ using the mean-field approximation. In particular, we analyze magnetic phase transitions to characterize the transition between ferromagnetic and paramagnetic states. We also study the magnetocaloric effect, including variations in magnetic entropy ΔS_m and relative cooling power RCP, to assess the material's potential for magnetic refrigeration applications. Finally, we examine the hysteresis behavior, focusing on coercivity, remanent magnetization and changes in the hysteresis loop as a function of temperature and applied magnetic field. The article is organized as follows: Section 2 presents the theoretical model and methodology, Section 3 discusses the results in detail, and Section 4 summarizes the key conclusions.

2. MODEL AND OGUCHI APPROXIMATION

In this work, we develop a theoretical model based on the mean-field approximation to investigate the magnetic and magnetocaloric properties as well as the hysteresis behavior of the antiperovskite compound $ZnFe_3C$. The crystalline structure of $ZnFe_3C$ is depicted in Fig. 1. In this structure, only Fe atoms are magnetic, each possessing a spin of $S = 5/2$.

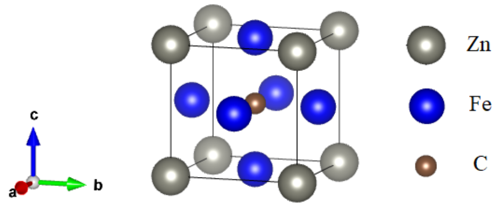

Fig. 1 – Crystal structure of $ZnFe_3C$ antiperovskite.

The Hamiltonian describing the antiperovskite is written as follows:

$$H = -J_1 \sum_{\langle i,j \rangle} S_i S_j - J_2 \sum_{\langle i,m \rangle} S_i S_m - h \sum_{i=1}^{N} S_i. \tag{1}$$

where J_1 and J_2 represent the exchange interactions between the spins of the first and second neighbors of the Fe^{3+} ions, respectively, and h is the external magnetic field applied to the spins of the system. Finally, N indicates the total number of sites.

To study the magnetic and magnetocaloric properties, as well as the hysteresis behavior of the $ZnFe_3C$ compound, we use the mean-field approximation, which simplifies the modeling of spin interactions by averaging them. Although this approach does not take into account certain short-range correlations, it remains suitable for modeling global magnetic behaviors.

Our method uses the Gibbs-Bogoliubov inequality to obtain an estimate of the free energy [30]:

$$F(H) \leq F_0(H_0) + \langle H - H_0 \rangle_0 \equiv \Phi, \tag{2}$$

where F and F_0 are the free energies of two systems, described respectively by the Hamiltonian H (1) and the trial Hamiltonian H_0 (3). The thermal mean $\langle H - H_0 \rangle_0$ is calculated on the set associated with H_0.

The trial Hamiltonian H_0 used in this study is expressed simply as follows:

$$H_0 = -L \sum_{i=1}^{N} S_i, \tag{3}$$

where L denotes the variational parameter related to spin S.

From this trial Hamiltonian H_0 (3), the partition function Z_0 is calculated as follows:

$$Z_0 = Tr(e^{-\beta H_0}) = \left[2\cosh\left(\frac{5}{2}\beta L_0\right) + 2\cosh\left(\frac{3}{2}\beta L_0\right) + 2\cosh\left(\frac{1}{2}\beta L_0\right) \right]^N, \tag{4}$$

where $\beta = 1/k_B T$, $k_B = 1$ being Boltzmann's constant and T is the absolute temperature.

From the equation for the partition function Z_0, we can easily deduce the expression for the free energy F_0:

$$F_0 = -\frac{\ln(Z_0)}{\beta} = -\frac{N}{\beta} \ln\left[2\cosh\left(\frac{5}{2}\beta L_0\right) + 2\cosh\left(\frac{3}{2}\beta L_0\right) + 2\cosh\left(\frac{1}{2}\beta L_0\right) \right]. \tag{5}$$

From (5) and applying the Gibbs-Bogoliubov inequality (2), we obtain the analytical expression for the free energy Φ:

$$\frac{\Phi}{N} = -\frac{1}{\beta} \ln\left[2\cosh\left(\frac{5}{2}\beta L\right) + 2\cosh\left(\frac{3}{2}\beta L\right) + 2\cosh\left(\frac{1}{2}\beta L\right) \right] - 4J_1 M^2 - 3J_2 M^2 - hM + LM, \tag{6}$$

where $M = \langle S_i \rangle$ represents the magnetization per site.

Minimizing this free energy (6) yields the expressions for the variational and order parameters:

$$L = 8J_1 M + 6J_2 M + h, \tag{7}$$

$$M = \frac{5\sinh(\frac{5}{2}\beta L) + 3\sinh(\frac{3}{2}\beta L) + \sinh(\frac{1}{2}\beta L)}{\cosh(\frac{5}{2}\beta L) + \cosh(\frac{3}{2}\beta L) + \cosh(\frac{1}{2}\beta L)}. \tag{8}$$

The magnetic susceptibility of the system, χ, is defined by the derivative of the magnetization M (8) with respect to the external magnetic field h :

$$\chi = \frac{\partial M}{\partial h}\Big]_{h=0}. \tag{9}$$

Using Maxwell's thermodynamic relation, the magnetic entropy variation $\Delta S_m(T,h)$ for an external magnetic field varying from 0 to h can be formulated as follows [31, 32]:

$$\Delta S_m(T,h) = \int_0^h \left(\frac{\partial M}{\partial T}\right)_{h_i} dh_i, \tag{10}$$

where $\frac{\partial M}{\partial h}$ represents the magnetization under the effect of a specific external magnetic field h_i.

For measurements taken at discrete values of external magnetic field h and temperature T, this magnetic entropy variation $\Delta S_m(T,h)$ is often approximated by a discrete sum:

$$\Delta S_m(T,h) = \sum_i \frac{M_{i+1} - M_i}{T_{i+1} - T_i} \Delta h_i, \tag{11}$$

where M_{i+1} and M_i represent the magnetizations measured under an external magnetic field h, at temperatures T_{i+1} and T_i respectively.

The relative cooling capacity (RCP) is quantified using the following formula:

$$RCP = -\Delta S_m^{max}.\delta T_{FWHM}, \tag{12}$$

where $-\Delta S_m^{max}$ corresponds to the peak of the isothermal magnetic entropy variation, and δT_{FWHM} is the width at mid-height of the temperature range around the peak.

To simplify calculations, we adopt the exchange interactions J_1 and J_2 as units, setting them at $J_1 = J_2 = 1$. This normalization facilitates analysis of the influence of the external magnetic field and temperature on the magnetic and magnetocaloric properties of the system. In general, solutions to the mean-field equation (8) are not necessarily unique. However, the physically significant solutions, *i.e.* those that describe stable equilibrium phases, are those that minimize the free energy (6). This minimization guarantees that the system reaches a thermodynamically favorable state, in accordance with the principles of statistical mechanics. It should also be noted that the mean field equation (8) was solved using the Fortran 90 programming language. This choice was motivated by the language's robustness in handling intensive numerical calculations and its ability to deliver fast, accurate results for complex systems.

3. RESULTS AND DISCUSSION

Figure 2 shows the variation of magnetization (M) as a function of temperature (T) in the absence of an external magnetic field ($h = 0$) for the antiperovskite compound $ZnFe_3C$. Initially, the magnetization starts at its saturation value ($M = 2.5$) and then gradually decreases with increasing temperature until it reaches zero ($M = 0$) in the paramagnetic phase. This behavior indicates a second-order phase transition between the ferromagnetic and paramagnetic phases, with a critical temperature of $T_c = 41$. This phenomenon can be explained by the fact that, at low temperatures, the magnetic moments are strongly aligned due to ferromagnetic exchange interactions between the spins in the system. However, as the temperature increases, thermal fluctuations disrupt this alignment, leading to a decrease in magnetization.

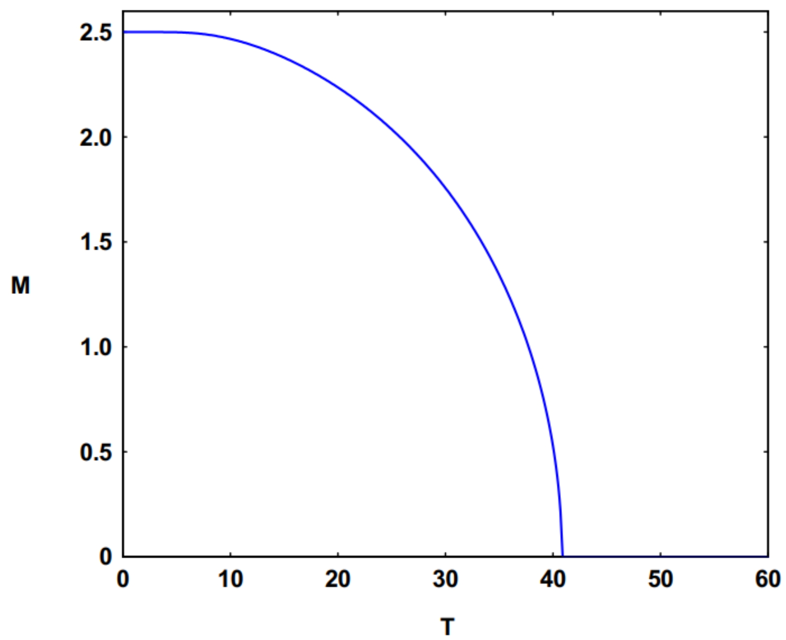

Fig. 2 – The variation of magnetization M as a function of temperature T.

To complete the magnetization plot, Fig. 3 illustrates the thermal variation of the magnetic susceptibility χ of our studied system, in the absence of the external magnetic field. A marked susceptibility peak can be observed at the critical temperature, highlighting the transition point between the ferromagnetic and paramagnetic phases. This behavior has already been observed in other studies [33, 34]. Interestingly, the maximum magnetic susceptibility shown in Fig. 3 corresponds to the critical temperature T_c, which marks the transition between the ferromagnetic and

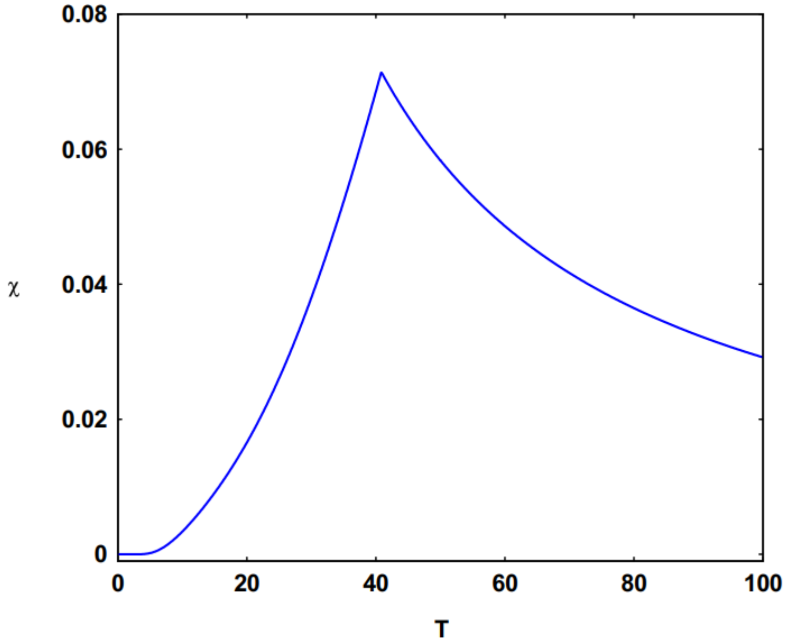

Fig. 3 – The variation of magnetic susceptibility χ as a function of temperature T.

paramagnetic phases. At this temperature, the system reaches maximum sensitivity to thermal fluctuations, highlighting the instability of the spins as they move from an ordered to a disordered state. This peak is an essential thermodynamic signature of the magnetic phase transition.

To analyze the influence of the external magnetic field (h) on the magnetization (M) and transition temperature (T_c), Fig. 4 presents the variation of magnetization (M) as a function of temperature (T) for different external magnetic field strengths ($h = 1$, 2, 3, 4, and 5). The results show that an increase in the external magnetic field leads to an increase in the critical temperature (T_c). Physically, this can be explained by the stabilizing effect of the external magnetic field on the ferromagnetic order, which strengthens the alignment of magnetic moments. A stronger field requires more thermal energy (higher temperature) to disrupt this alignment and transition to the paramagnetic phase. Additionally, for all values of h, the magnetization decreases progressively and tends toward zero as the critical temperature (T_c) is approached. At higher temperatures, the magnetization becomes negligible regardless of the applied field strength, indicating the system's transition to the paramagnetic phase where magnetic moments are randomly oriented. These observations are consistent with results reported in other studies [35–37]. The influence of the external magnetic field (h) on the magnetic susceptibility (χ) is illustrated in Fig. 5.

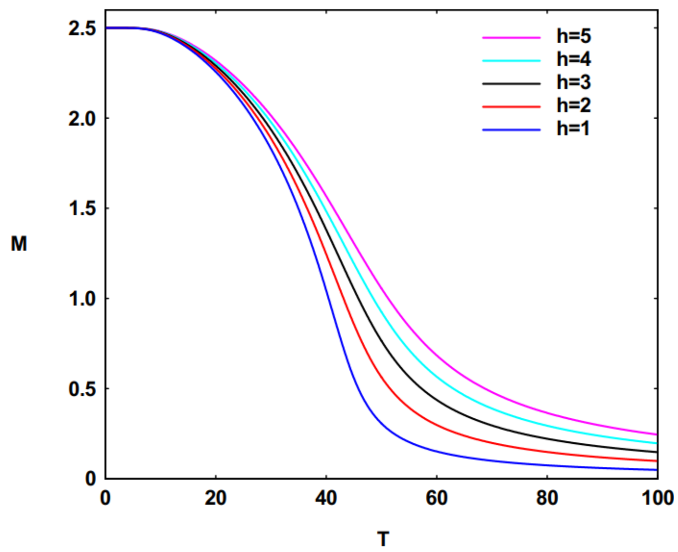

Fig. 4 – The variation of magnetization M as a function of temperature T for different values of external magnetic field h.

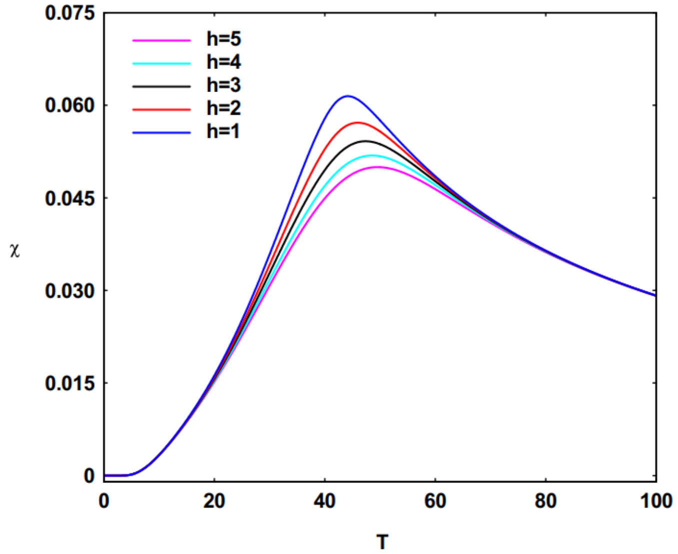

Fig. 5 – The variation of magnetic susceptibility χ as a function of temperature T for different values of external magnetic field h.

The results show that the peaks of χ occur at the critical temperature (T_c), marking the system's transition from the ferromagnetic to the paramagnetic phase. At this point, the system becomes particularly sensitive to thermal fluctuations, leading to the appearance of these peaks. However, as the external magnetic field increases, the intensity of these peaks decreases. A higher magnetic field stabilizes the alignment of magnetic moments, reducing the impact of thermal fluctuations around T_c and making the phase transition less pronounced. Figure 6 presents the magnetic entropy

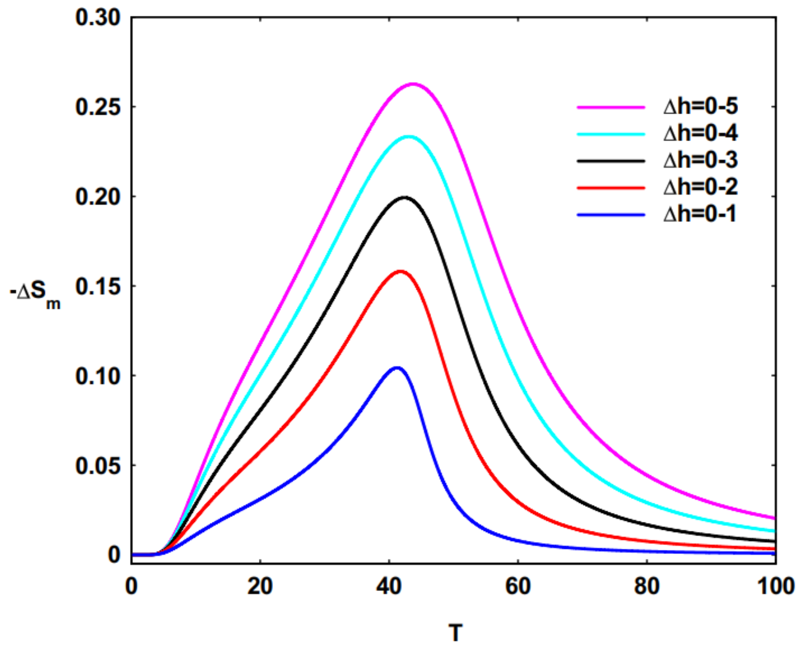

Fig. 6 – Magnetic entropy change $-\Delta S_m$ as a function of temperature T for different values of external magnetic field h.

change ($-\Delta S_m$) of the antiperovskite compound $ZnFe_3C$ as a function of temperature (T) for various external magnetic field strengths. The results show that $-\Delta S_m$ increases with temperature, reaching a peak at the critical temperature (T_c), and then decreases beyond this point. The peak corresponds to the phase transition from the ordered ferromagnetic phase to the disordered paramagnetic phase. Additionally, increasing the external magnetic field strength increases the maximum value of $-\Delta S_m$, which rises from 0.10 for $\Delta h = 1$ to 0.26 for $\Delta h = 5$. This can be attributed to the alignment of magnetic moments under the applied field at low temperatures, which reduces entropy. At T_c, the system undergoes a significant entropy change, reflecting the phase transition. Above T_c, thermal agitation dominates, leading to disorganization of magnetic moments and diminishing the magnetocaloric effect.

These results suggest that $ZnFe_3C$ is a promising material for magnetic refrigeration applications near T_c, comparable to findings in other studies [33, 38, 39]. Figure 7

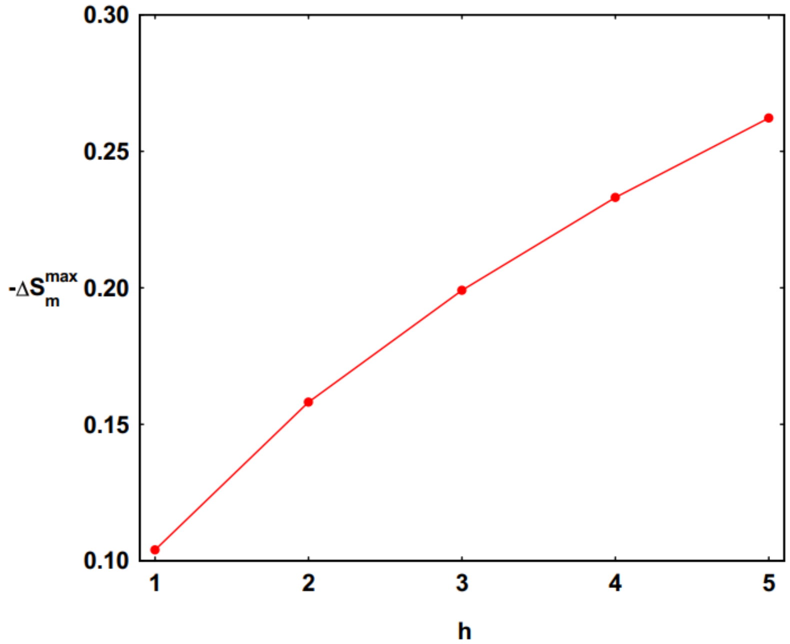

Fig. 7 – Maximum magnetic entropy change $-\Delta S_m^{max}$ as a function of external magnetic field h.

illustrates the maximum magnetic entropy change ($-\Delta S_m^{\max}$) as a function of external magnetic field strength (h). The results show a clear linear increase in $-\Delta S_m^{\max}$ with increasing h, which is characteristic of a second-order magnetic phase transition. This linearity indicates that in this type of transition, the magnetic entropy change responds proportionally to the applied field strength, without abrupt changes, reflecting the continuity in the variation of the material's magnetic properties. Figure 8 shows that the maximum value of $-\Delta S_m^{\max}$ increases linearly with the two-thirds power of the applied external magnetic field ($h^{2/3}$), confirming the second-order phase transition nature of the system. For materials undergoing a second-order transition, this linear relationship between $-\Delta S_m^{\max}$ and $h^{2/3}$ is typical, reflecting a continuous evolution of the material's magnetic properties near T_c. This behavior highlights the predictive nature of the response to external fields, reinforcing the idea of a smooth phase transition characteristic of second-order transitions. Figure 9 illustrates the variation of relative cooling power (RCP) as a function of external magnetic field strength (h) for values ranging from 1 to 5. RCP serves as a key parameter for evaluating the performance of magnetocaloric materials in magnetic cooling applications. The

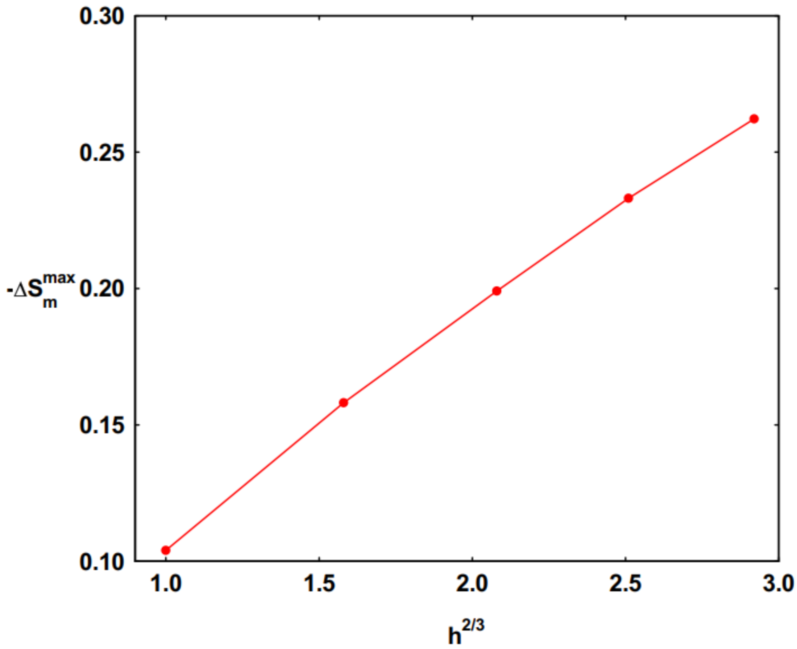

Fig. 8 – Maximum magnetic entropy change $-\Delta S_m^{max}$ with respect to the two third of external magnetic field $h^{2/3}$.

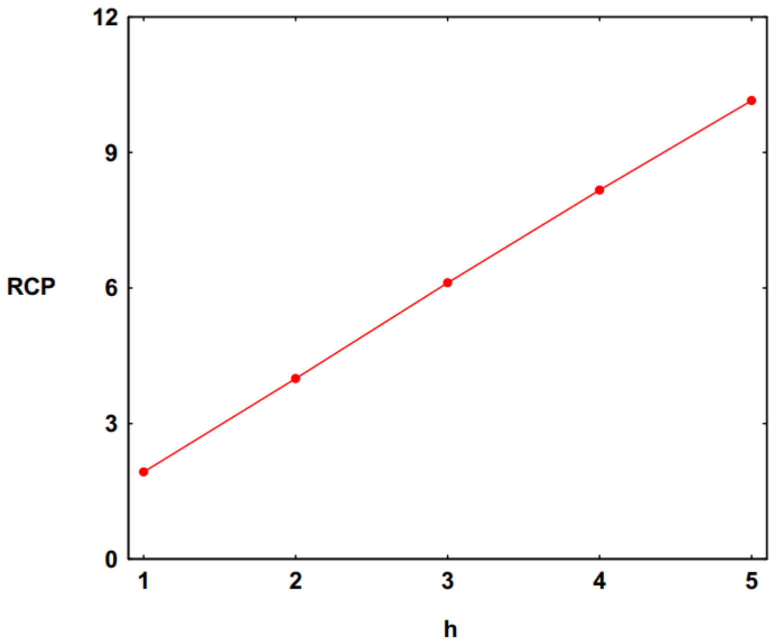

Fig. 9 – Relative cooling power RCP as a function of external magnetic field h.

results reveal a linear increase in RCP with increasing field strength, suggesting that $ZnFe_3C$ possesses favorable properties for use in magnetic cooling devices. This linear trend indicates that the efficiency of the material improves with increasing field strength, further underscoring its potential for energy-efficient cooling systems. Similar linear behavior of RCP as a function of field strength has been reported in other studies [33, 38, 39].

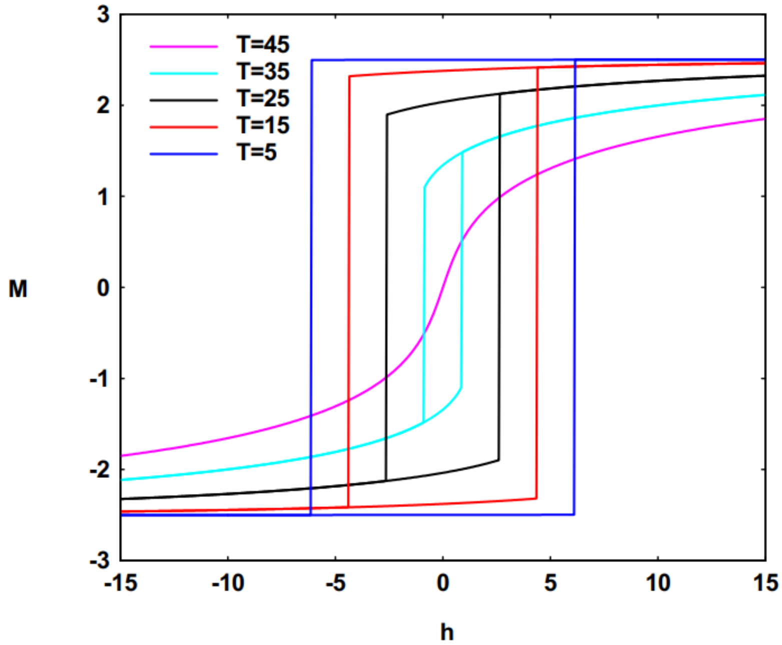

Fig. 10 – The magnetic hysteresis loop of the antiperovskite compound $ZnFe_3C$.

To study the effect of temperature on hysteresis behavior, Fig. 10 presents the variation of magnetization (M) as a function of the external magnetic field (h) at different temperatures ($T = 5$, 15, 25, 35, and 45). It can be observed that as the temperature increases, the surface area of the hysteresis loop progressively decreases. This behavior is attributed to the increase in thermal agitation, which disturbs the alignment of magnetic moments in the system. At low temperatures, the magnetic moments remain well-aligned, resulting in a pronounced hysteresis loop. However, at higher temperatures, increased thermal agitation disrupts this alignment, reducing the amplitude of the hysteresis loop. When the temperature exceeds the critical temperature ($T_c = 41$), the thermal energy becomes sufficient to completely disorganize the magnetic moments, causing the hysteresis loop to vanish and signaling the transition to the paramagnetic state. Similar temperature-dependent hysteresis behavior has been reported in Refs. [40–44]. It is important to note that the rectangular hysteresis loop observed in this study, which cannot be measured experimentally for a magnetic system, can be explained by several factors. It may be a theoretical prediction resulting from a simplified model, such as the mean-field approximation, which neglects effects such as short-range correlations, disorder or dissipative processes such as spin-lattice interactions. In a real material, these phenomena generate more gradual magnetization transitions and energy losses, making a perfectly rectangular loop inaccessible. In addition, instrumental limitations, such as the strength of available magnetic fields or the temporal resolution of measurements, may prevent the observation of these abrupt transitions. This form of hysteresis loop has, however, been widely observed in other theoretical work, showing that it is often the result of simplifications inherent in idealized models. It is also important to note that the hysteresis loop obtained in this study is predicted at low temperature, whereas experiments are generally carried out at room temperature, which could also explain this difference. For a more detailed analysis of the effect of temperature (T) on the

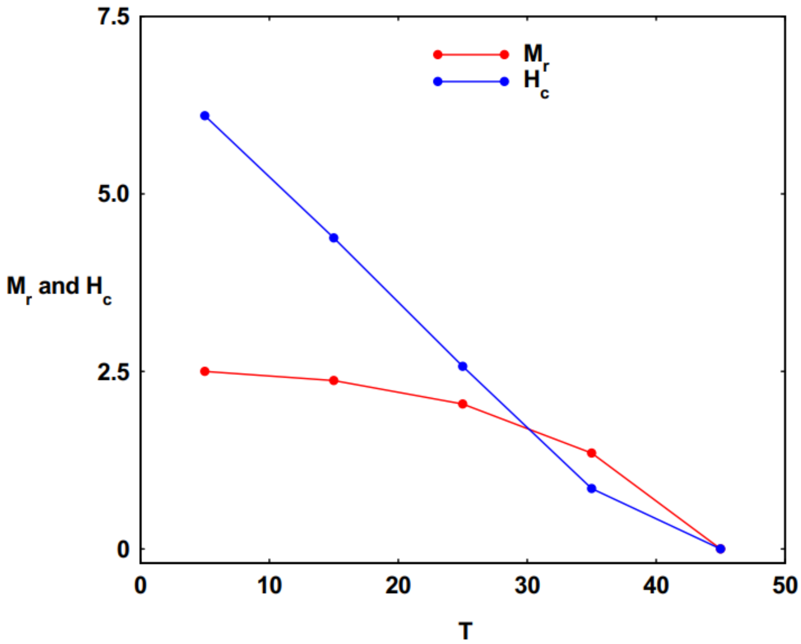

Fig. 11 – Effect of the temperature T on the coercivity H_c and the remanence M_r of the antiperovskite compound $ZnFe_3C$.

coercivity (H_c) and remanence (M_r), Fig. 11 illustrates the variation of these two hysteretic parameters as functions of temperature. It is evident that as T increases, both H_c and M_r decrease progressively. This trend reflects the reduced alignment of magnetic moments due to the influence of increasing thermal agitation, which diminishes the compound ability to sustain remnant magnetization and high coercivity at elevated temperatures.

4. CONCLUSION

In this study, we investigated the magnetic and magnetocaloric properties of the $ZnFe_3C$ compound using the mean-field approximation. Our results show that the critical temperature (T_c) increases with a stronger external magnetic field. The magnetic entropy change ($-\Delta S_m$), which peaks at T_c, confirms a significant magnetocaloric effect. Additionally, the relative cooling power (RCP) increases linearly with the strength of the applied magnetic field. Hysteresis analysis demonstrates a gradual reduction in coercivity and remanence as temperature increases, with the hysteresis loop disappearing above T_c, indicating the transition to the paramagnetic phase. These findings highlight the potential of $ZnFe_3C$ as a promising material for sustainable and high-performance magnetic refrigeration systems.

REFERENCES

1. H. Kerrai, A. Zaim, M. Kerouad, Magnetocaloric effect in the full-Heusler alloy Ga_2MnNi for magnetic refrigeration: A first-principles and Monte Carlo study, *Phys. Status Solidi-Rapid Res. Lett.* **19**, 2400294 (2025).
2. E.M. Jalal, H. Kerrai, H. Saadi, N. Hachem, A. Hasnaoui, M. El Bouziani, Theoretical investigation of magnetic and magnetocaloric properties of the half-Heusler alloy MnCoBi for magnetic refrigeration applications, *Phys. Lett. A* **527**, 130007 (2024).
3. H. Kerrai, H. Saadi, E.M. Jalal, M. Kerouad, A. Zaim, Hysteresis behavior and magnetocaloric effect in $MnNiGa_2$ full-Heusler alloy, *Solid State Commun.* **394**, 115717 (2024).
4. A. Kitanovski, Energy applications of magnetocaloric materials, *Adv. Energy Mater.* **10**, 1903741 (2020).
5. H. Kerrai, N. Zaim, M. Kerouad, A. Zaim, Insight into electronic and magnetic properties of Ba_2NiOsO_6 double perovskite: A Monte Carlo study and a comparative investigation between TB-mBJ and GGA+U, *Comput. Mater. Sci.* **246**, 113404 (2025).
6. E. Warburg, Magnetische Untersuchungen, *Ann. Phys.* **249**, 141-164 (1881).
7. L. Li, M. Yan, Recent progresses in exploring the rare-earth-based intermetallic compounds for cryogenic magnetic refrigeration, *J. Alloy. Compd.* **823**, 153810 (2020).
8. G.B. Huang, C.X. Chang, X.F. Wu, Y.S. Du, G. Fu, L. Ma, L. Li, G. Cheng, J. Wang, J.T. Zhao, G.H. Rao, Successive magnetic transitions and magnetocaloric effects in intermetallic compounds RE_5Pt_3 (RE = Dy, Ho), *Mater. Res. Bull.* **172**, 112663 (2024).
9. V.K. Pecharsky, K.A. Gschneidner, Effect of alloying on the giant magnetocaloric effect of $Gd_5(Si_2Ge_2)$, *J. Magn. Magn. Mater.* **167**, L179-L184 (1997).
10. O. Tegus, E. Brück, K.H.J. Buschow, F.R. de Boer, Transition-metal-based magnetic refrigerants for room-temperature applications, *Nature* **415**, 150-152 (2002).
11. F.X. Hu, B.G. Shen, J.R. Sun, Z.H. Cheng, G.H. Rao, X.X. Zhang, Influence of negative lattice expansion and metamagnetic transition on magnetic entropy change in the compound $LaFe_{11.4}Si_{1.6}$, *Appl. Phys. Lett.* **78**, 3675-3677 (2001).

12. H. Wada, Y. Tanabe, Giant magnetocaloric effect of $MnAs_{1-x}Sb_x$, *Appl. Phys. Lett.* **79**, 3302-3304 (2001).
13. Z. Quan, W. Liu, H. Hu, S. Xu, B. Sebo, G. Fang, M. Li, and X. Zhao, Microstructure, electrical and magnetic properties of Ce-doped $BiFeO_3$ thin films, *J. Appl. Phys.* **104**, 084106 (2008).
14. Y.Y. Shu, L.F. Wang, S.L. Huang, Y.K. Zhang, Magnetic properties and large magneto-caloric effect in the amorphous $Ho_{0.2}Tm_{0.2}Gd_{0.2}Co_{0.2}Al_{0.2}$ ribbon, *J. Non Cryst. Solids* **628**, 122846 (2024).
15. Y. Zhang, W. Hao, J. Shen, Z. Mo, T. Gottschall, L. Li, Investigation of the structural and magnetic properties of the GdCoC compound featuring excellent cryogenic magnetocaloric performance, *Acta Mater.* **276**, 120128 (2024).
16. Y. Zhang, Y. Xie, J. Wei, and W. Hao, Experimental and theoretical insights into the structural, magnetic, and low-temperature magnetocaloric properties of RE_2CoTiO_6 (RE = Gd, Dy, and Er) double perovskite oxides, *J. Mater. Chem. A* **12**, 32396-32407 (2024).
17. Z. Zhang, G. Yao, L. Zhang, P. Jia, X. Fu, W. Cui, Q. Wang, Magnetic phase transition and room-temperature magnetocaloric effects in $(Al,M)Fe_2B_2$ (M = Si, Ga) compounds, *J. Magn. Magn. Mater.* **484**, 154-158 (2019).
18. J. Lin, X. Wang, F. Chen, H.-F. Li, L. Li, Designing Gadolinium-Transition Metals-Based Perovskite Type High Entropy Oxides with Good Cryogenic Magnetocaloric Performances, *J. Mater. Sci. Technol.* **207**, 317-323 (2025).
19. Z. Li, D. Ding, L. Xia, Excellent magneto-caloric effect of a binary $Gd_{63}Ni_{37}$ amorphous alloy, *Intermetallics* **86**, 11-14 (2017).
20. Y. Zhang, W. Hao, J. Lin, H. Li, L. Li, Geometrically frustrated $Gd_2Ti_2O_7$ oxide: A comprehensive exploration of structural, magnetic, and magnetocaloric properties for cryogenic magnetic cooling applications, *Acta Mater.* **272**, 119946 (2024).
21. Y. Zhang, W. Hao, J. Shen, Z. Mo, T. Gottschall, L. Li, Investigation of the structural and magnetic properties of the GdCoC compound featuring excellent cryogenic magnetocaloric performance, *Acta Mater.* **276**, 120128 (2024).
22. F. Chen, Y. Na, Y. Xie, Y. Zhang, Insight into the structural and magnetic properties of PrZnSi and NdZnSi compounds featuring large low-temperature magnetocaloric effects, *ACS Appl. Mater. Interfaces* **16**, 52719 (2024).
23. H. Kerrai, A. Zaim, M. Kerouad, Magnetic and magnetocaloric effect of Ba_2FeReO_6 double perovskite: Ab-initio and Monte Carlo studies, *Vacuum* **222**, 113090 (2024).
24. W. Chen, Y. Na, F. Chen, Y. Zhang, Cryogenic magnetic and magnetocaloric properties in anhydrous rare-earth sulfate $RE_2(SO_4)_3$ (RE= Tb, Dy, Ho, Er), *Cryogenics* **146**, 104012 (2025).
25. Ran Ji, Yangzhou Du, Xinpeng Na, Xin Wang, Lingwei Li, Investigation of the structural and cryogenic magnetic properties in Gd_2CrCoO_6 oxide, *Inorg. Chem. Commun.* **174**, 113964 (2025).
26. H. Kerrai, A. Zaim, M. Kerouad, First-principles study of the structural, magnetic and optoelectronic properties of double perovskite Ba_2FeReO_6, *Phys. Scr.* **99**, 075983 (2024).
27. Y. Zhang, J. Y. Law, A. Li, W. Hao, V. Franco, L. Li, Unveiling the Structural, Electronic and Magnetic Properties of $Gd_{4.5}A_{0.5}Si_3O_{13}$ (A = K, Na, and Li) Oxides With Promising Potential for Low-Temperature Magnetic Cooling, *Small* **21**, 2409981 (2024).
28. H. Kerrai, A. Zaim, M. Kerouad, Structural, Electronic, and Magnetic Properties of Ferrimagnetic Double-Perovskite Ba_2GdRuO_6: Density Functional Theory and Monte Carlo Simulation, *Phys. Status Solidi-Rapid Res. Lett.* **19**, 2400330 (2025).
29. M. Hajjami, A. Oubelkacem, Y. Benhouria, M. Kibbou, I. Essaoudi, and A. Ainane, The structural, electronic and magnetic properties of Fe_3ZnC anti-perovskite, *Chin. J. Phys.* **91**, 575–582 (2024).
30. H. Falk, Inequalities of JW Gibbs, *Am. J. Phys.* **38**, 858–869 (1970).

31. M. Balli, P. Fournier, S. Jandl, K.D. Truong, and M.M. Gospodinov, Analysis of the phase transition and magneto-thermal properties in La_2CoMnO_6 single crystals, *J. Appl. Phys.* **116**, 073907 (2014).
32. K.A. Gschneidner, V. K. Pecharsky and A.O. Tsokol, Recent developments in magnetocaloric materials, *Rep. Prog. Phys.* **68**, 1479 (2005).
33. H. Kerrai, N. Zaim, M. Kerouad, A. Zaim, Ab-initio and Monte Carlo studies of magnetic and magnetocaloric properties of antiperovskite Mn_3AlN, *Comput. Mater. Sci.* **232**, 112648 (2024).
34. H. Kerrai, A. Zaim and M. Kerouad, Magnetic energy product and hysteresis behavior of antiperovskite Mn_3AlN: Monte Carlo Simulation, *Phys. Scr.* **99**, 065986 (2024).
35. M. Salama, E. M. Jalal, H. Saadi, H. Kerrai, N. Hachem, E. B. Choubabi, M. El Bouziani, Theoretical study of magnetic, magnetocaloric, and hysteresis behavior of the antiperovskite compound Mn_3AlN, *Appl. Phys. A* **131**, 155 (2025).
36. H. Kerrai, E. M. Jalal, A. Zaim, A. Hasnaoui, M. Kerouad, M. El Bouziani, Study of magnetic properties and phase diagrams of the full Heusler Ga_2MnCo alloy, *Appl. Phys. A* **130**, 816 (2024).
37. H. Kerrai, N. Zaim, M. Kerouad, and A. Zaim, Monte Carlo study of the phase diagrams and hysteresis behaviors of a ternary mixed spin-(1, 1/2, 3/2) Ising nanowire with ferromagnetic core/ferrimagnetic shell structure, *Physica B: Condensed Matter* **649**, 414448 (2024).
38. N. Ennassiri, N. Tahiri, O. El Bounagui, H. Ez-Zahraouy, and A. Benyoussef, Magnetic, magnetocaloric and transport properties in $AlCMn_3$ antiperovskite compound, *J. Alloys Compd.* **741**, 1196-1202 (2018).
39. N. Ennassiri, N. Tahiri, O. El Bounagui, H. Ez-Zahraouy, and A. Benyoussef, Structural, electronic, magnetic, and magnetocaloric properties in metallic antiperovskite compound Mn_3GaC, *Mater. Res. Bull.* **98**, 335–339 (2018).
40. H. Kerrai, N. Zaim, M. Kerouad, and A. Zaim, Magnetic and electronic properties of double perovskite Sr_2CrMoO_6 for spintronic applications: insights from first-principles and Monte Carlo approaches, *Commun. Theor. Phys.* **76**, 125701 (2024).
41. M. Salama, E. Dahbani, Y. Al Qahoom, E.B. Choubabi, N. Hachem, and M. El Bouziani, Magnetic properties and compensation temperatures of a graphene bilayer by Monte Carlo simulation, *Physica B* **684**, 415987 (2024).
42. N. Zaim, H. Kerrai, M. Zaim, M. Kerouad, A. Zaim, Dynamic hysteresis behaviors of a graphene nanoribbon with a mixed spin-5/2 and 2 under the influence of a time-varying magnetic field, *Vacuum* **228**, 113536 (2024).
43. M. Salama, T. Mouhrach, E.B. Choubabi, N. Hachem, and M. El Bouziani, Mean-field study of magnetic properties and hysteresis behavior in a bilayer graphene Ising system, *Phys. Scr.* **99**, 055917 (2024).
44. H. Saadi, A. Al-Rajhi, E.M. Jalal, O. Hachem, M. Madani, M. El Bouziani, Monte Carlo simulation of the magnetic properties of a multilayer mixed-spin system (5/2, 3/2), *Vacuum* **232**, 113781 (2025).